1. Self-Organized Criticality Phenomena

How can the universe start with a few types of elementary particles
at the big bang, and end up with life, history, economics, and literature?
The question is screaming out to be answered but it is seldom even asked.
Why did the big bang not form a simple gas of particles, or condense into one big crystal ?

Per Bak (1996), *How Nature Works*

In this introductory chapter we want to get a flavor of physical processes that are governed by self-organized criticality, starting from small experiments in our laboratories, proceeding to nature phenomena on our planet, all the way to the remotest astrophysical realms of our universe. We will discover that most complex systems with many interacting components display some nonlinear behavior that is governed by self-organized criticality. The remainder of the book will focus on numerical, analytical, and physical modeling of self-organized criticality in astrophysical systems.

1.1 The Concept of Self-Organized Criticality

This book is all about nonlinear systems in nature. What do we mean by a "system"? A *system* is a set of interacting (or interdependent) components or entities that are combined into an integrated whole, such as a car (a mechanical system), a coupled pendulum (a physical system), tectonic plates (a geological system), a hurricane (a weather system), the stock market (an economic system), or an accretion disk in a binary star system (an astrophysical system).

Our whole universe is governed by nonlinear systems or nonlinear dynamics. In principle, a system can exhibit linear or nonlinear behavior, depending on how the output is causally related to the input of the system. The property of linearity is well-defined in mathematics: a linear function (or equation) obeys the properties of additivity, $f(x+y) = f(x) + f(y)$, and homogeneity, $f(a \times x) = a \times f(x)$. A car, for instance, is a linear mechanical system by design: the directional change of the wheels is proportional

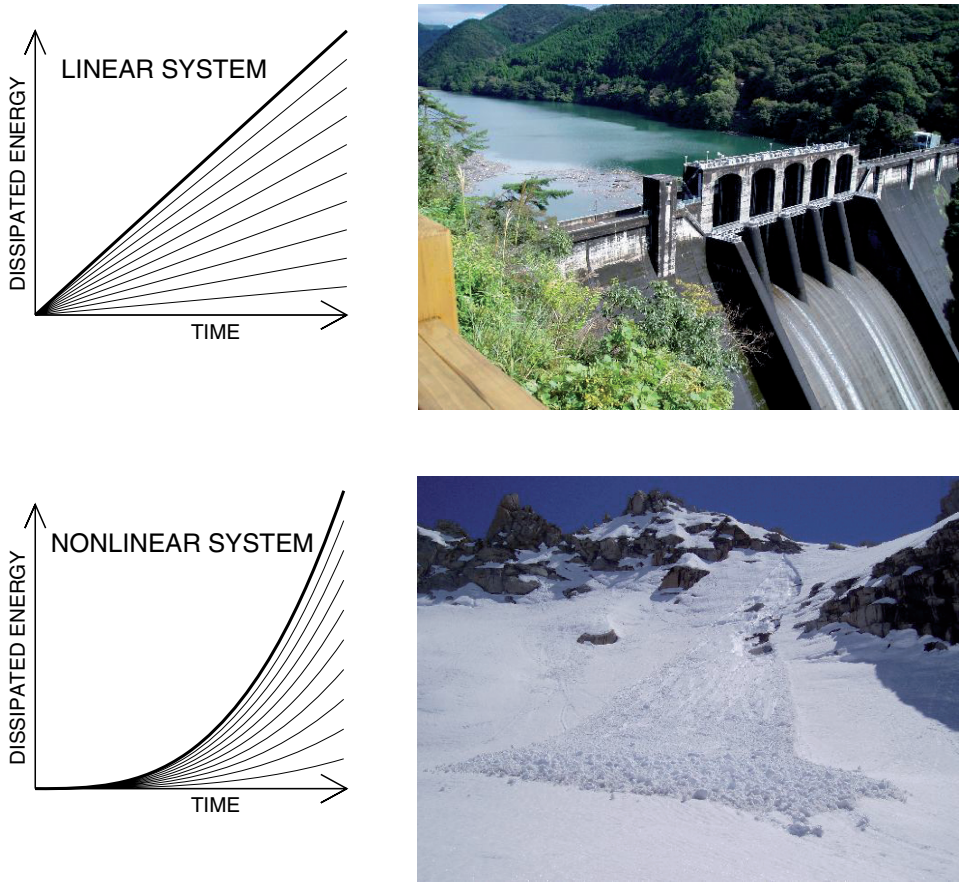

Fig. 1.1 The output or dissipated energy in a linear system grows linearly with time, for a constant input rate (top left), while the output is highly unpredictable and not correlated with the input rate in a nonlinear dissipative system (bottom left). A practical example of a linear system is a hydroelectric plant, where the produced electric energy is proportional to the water input, as depicted by the water-storage dam at Yaotsu, Gifu, Japan (top right). A classical example of a dissipative nonlinear system is a snow avalanche, as shown in the large wet-snow avalanche at Deadman Canyon in the Sierra Nevada range (bottom right).

to the angle you turn on the steering wheel. Also a hydropower plant can be described as a linear system, since the produced electric energy is proportional to the water input that flows out of a dam into the pipeline of the power plant (Fig. 1.1, top). The electric output of multiple power plants requires a proportional amount of water supply, so the properties of additivity and homogeneity typical for linear systems is fulfilled. Of course, the linear behavior occurs only in a limited parameter range.

Many systems, however, consist of a large number of entities that interact in a complex way and exhibit nonlinear behavior, which are called *nonlinear dissipative systems*, such as coupled pendulums, avalanches (Fig. 1.1, bottom), earthquakes, hurricanes, the stock market, or star-forming molecular clouds. Coupled pendulums pull and kick each

other with rapidly changing amplitudes and phases, so that the resulting motion becomes chaotic (for a discussion of chaotic systems see Section 10.7). Tectonic plates have complicated interactions with cracking, shearing, or sliding motions, so that earthquakes happen at very irregular time intervals. A hurricane originates far out in the ocean as a result of apparently insignificant fluctuations of thermal gradients, air pressure, and circular motions, which evolve into powerful monsters that amass more and more angular momentum until they cause a catastrophe at landfall. Edward Lorenz, a pioneer of chaos theory, coined the term *"butterfly effect"* (inspired by a 1952 science fiction story by Ray Bradbury), which refers to the idea that a butterfly's wing flap might be sufficient to cause a change in the atmosphere that ultimately could result in a tornado. The stock market can behave quite regularly over many days, but sporadic glitches that lead to a Wall Street crash can happen unpredictably. Molecular clouds in our galaxy condense as a result of angular momentum and gravity (or triggered by a supernova shock), until a gravitational collapse sets in and leads to star formation. So, there are many nonlinear dissipative systems in our universe, which exhibit inherent nonlinear behavior just as a result of complex interactions that occasionally lead to instabilities with subsequent catastrophes. However, although we humans pay most attention to the largest events, the catastrophes, the myriads of smaller events share the same statistical properties, which can be described with the concept of *self-organized criticality*.

What special condition is needed to enable self-organized criticality? Since there exists no *perpetuum mobile*, a system that works without external energy input ad infinitum, we obviously need a source of energy. This input of external energy often occurs randomly in nature, causing local disturbances of a system, to which a linear system will respond with a proportional change in output, while a nonlinear dissipative system will respond sporadically with a little or largely amplified output. A classical paradigm for self-organized criticality is a sandpile. If we continuously drip sand grains onto the same place, a conical sandpile will grow in a stable manner, with a steepening surface shape, until a critical slope (with an angle of $\approx$ 34–37 degrees, depending on the consistency, granularity, and humidity of the sand) is reached, after which the state of self-organized criticality sets in (Fig. 1.2, right panels). The continuously trickled sand will produce large or small avalanches of random sizes that have no relation to the input rate of sand (at least for low rates). This is the critical state that is needed to observe SOC phenomena. As long as the critical slope is not reached, the sand will be in a stable equilibrium, such as in the flat sand beach in northern California shown in Fig. 1.2 (left). So, we need two things, a continuous energy input source and a nonlinear dissipative system. The energy dissipation of sandpile avalanches corresponds to the kinetic energy and change in gravitational potential. The nonlinearity results from the highly complex interactions of colliding sand grains, which act on each other by collisions and friction. In contrast, water flowing through a pipeline (Fig. 1.1 top), has a much more linear characteristic, at least for laminar flows, because of the inherent physical properties of homogeneity and viscosity in fluids. Nonlinearity occurs in almost all systems with many components. The physics is only simple for one- or two-component systems, say under the influence of one gravitational or electric force (classical two-body descriptions), while the physical and mathematical treatment becomes immensely complex for n-body problems (for $n \geq 3$). In fluids, turbulence can already occur in a single fluid, and many instabilities can occur in two-fluid systems.

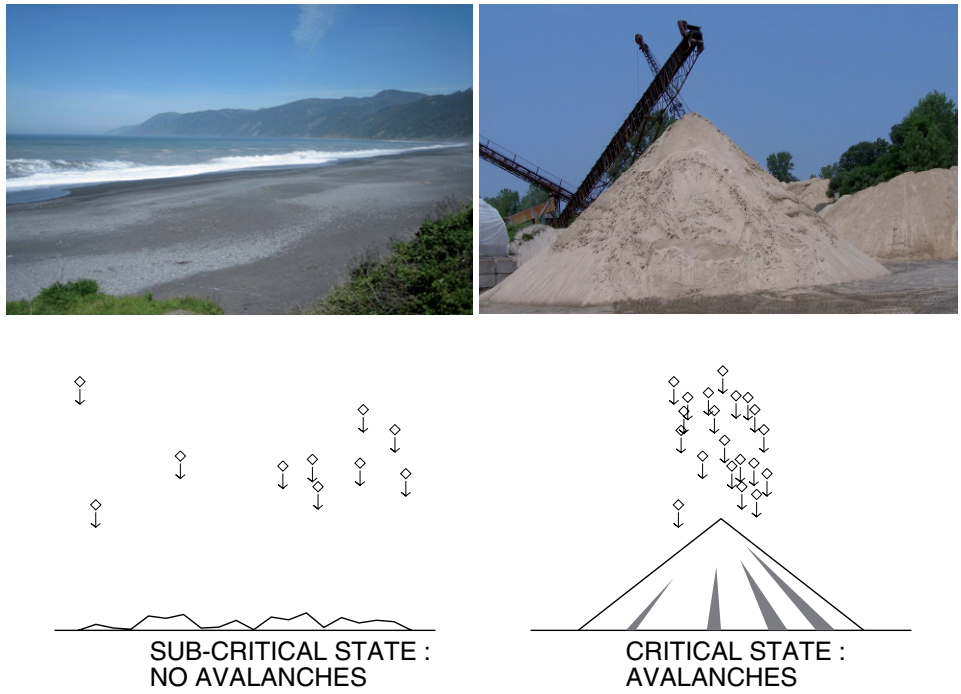

Fig. 1.2 A static equilibrium produces no avalanche events (bottom left panel), such as the flat sand beach in northern California (top left panel), while randomly dripping sand onto a sandpile produces a state of self-organized criticality where avalanches occur (bottom right panel), such as with the conveyer belt of the Indian River Enterprises (top right panel).

The concept of self-organized criticality has been pioneered by Per Bak and was first published in the seminal paper by Bak, Tang, and Wiesenfeld (1987), which has been cited already over 2000 times. Their brief abstract succinctly summarizes the quintessence of SOC: *We show that certain extended dissipative dynamical systems naturally evolve into a critical state, with no characteristic time or length scales. The temporal "fingerprint" of the self-organized critical state is the presence of 1/f noise; its spatial signature is the emergence of scale-invariant (fractal) structure.* The authors demonstrate the principle of SOC with a simple sandpile automaton model, which produces avalanches of arbitrary sizes that can be statistically sampled and exhibit a size distribution close to a powerlaw function. The powerlaw shape of size distributions became the hallmark and principal diagnostic of SOC phenomena (for which we will give a mathematical explanation in Chapter 3). However, as we will see later, powerlaw distributions are a necessary, but not a sufficient condition for SOC processes (Chapter 10; Sornette (2004), chapter 14 therein). Popular accounts of SOC phenomena can be found in the lucidly written book *How nature works* by Bak (1996), and in the article "Self-Organized Criticality" by Bak and Chen (1991) in *Scientific American*. Mathematical treatments of SOC phenomena can be found in the textbooks of Hendrik Jeldtoft Jensen (1998) and Didier Sornette (2004).

Before we proceed to practical examples of SOC phenomena, we should also clarify the difference between the terms *self-organization* and *self-organized criticality*. *Self-organization* refers to a broad range of pattern formation processes in both physical and biological systems. Pattern formation occurs through interactions internal to the system, without intervention of external directing influences (Camazine et al. 2001), such as zebra stripes, the bee's honeycomb structure, lichen growth, the hexagonal Bénard convection cells in boiling liquids, the granulation of the solar photosphere, in dusty space plasmas, or spheromaks. So, although the principle of *self-organization* is also concerned with complex interactions of neighboring components in a nonlinear system, it focuses on the resulting spatial (fractal) patterns, while the principle of *self-organized criticality* is concerned with the dynamical aspects. The dynamic behavior produces spatio-temporal events, whose statistical distributions of energy, temporal, and spatial scales can be sampled and quantitatively modeled.

1.2 SOC Laboratory Experiments

The principle of *self-organized criticality* was introduced by Bak, Tang, and Wiesenfeld (1987) as a theoretical concept, but the authors illustrated it also with the following practical example in the introduction of Bak et al. (1988): *To illustrate the basic idea of self-organized criticality in a transport system, consider a simple "pile of sand." Suppose we start from scratch and build the pile by randomly adding sand, a grain at a time. The pile will grow, and the slope will increase. Eventually, the slope will reach a critical value (called the "angle of repose"); if more sand is added it will slide off. Alternatively, if we start from a situation where the pile is too steep, the pile will collapse until it reaches the critical state, such that it is barely stable with respect to further perturbations.* At the end of their article, they suggest: *Finally, we invite the reader to perform the following home experiment. To demonstrate self-organized criticality, one needs a shoebox and a cup or two of sand – sugar or salt will do in a pinch. Wet the sand with a small amount of water, mix, and gather the sand into the steepest possible pile in one corner of the box. The angle of repose (i.e., the threshold slope) is larger for wet sand. So as the water evaporates, one observes a sequence of slides – some very small, others quite large – occurring at random places on the pile. (The evaporation process can be sped up by placing the box on a warm surface, or under direct sunlight.)*

Since experiments are always the toughest judge of new theories, several researchers started to test the SOC theory with sandpiles in their laboratory. The first experiment was performed by Jaeger et al. (1989) at the University of Chicago, who filled a cylindrical drum with grains, and rotated the drum slowly, like a concrete blender. Rotating the drum produces a one-sided sandpile with a critical slope inside the drum. The slow rotation steepens the slope and indeed created avalanches of all sizes. However, the authors did not find a powerlaw distribution of avalanche sizes. While the small-size and intermediate-size avalanches produced a powerlaw distribution, large-scale avalanches occurred in periodic time intervals when the slope became too steep. Bak (1996, p.68) blamed the failure to demonstrate SOC behavior in this experiment on the inertial effects of the rotation-induced periodic large-scale avalanches.

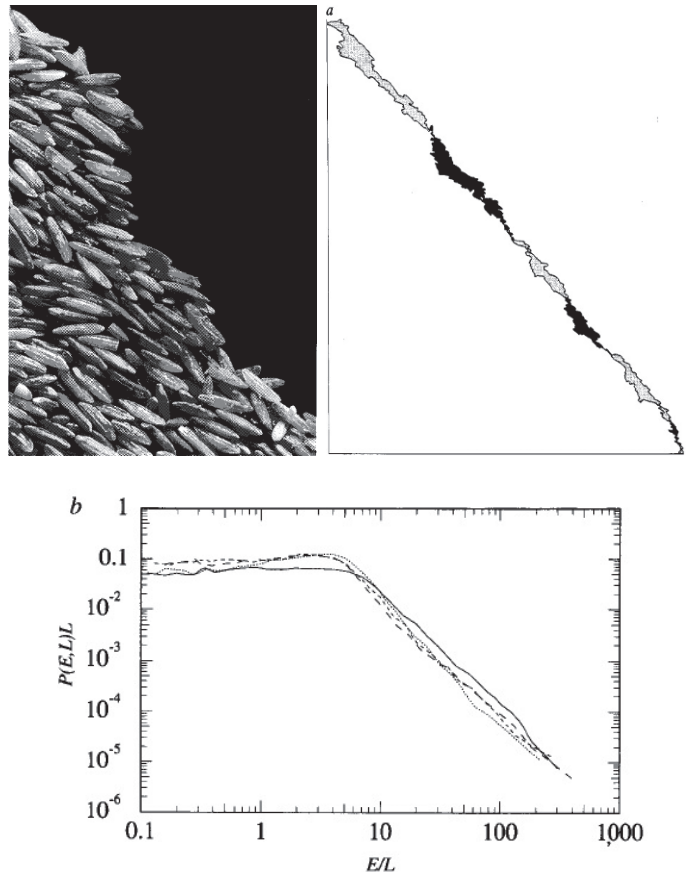

Fig. 1.3 The Norwegian rice pile experiment: a close-up photograph of a pile of rice, confined between two glass plates (top left); an electronically processed record of an avalanche, where loss and gains of rice mass is indicated with gray and black color (top right); and frequency distribution of the probability density $P(E,L)$ of events as a function of the energy dissipation E, normalized by the size L of the system. The powerlaw slope is $\alpha \approx 2.04$ (Frette et al. 1996).

A more accurate experiment closer to the suggestion of Bak et al. (1989) was carried out by Held et al. (1990) at IBM. They built a sandpile on top of a circular plate of an electronic precision scale. Sand grains were dropped slowly on top of the sandpile and the size of the resulting avalanche, if any, was recorded by the weight scale after each added sand grain. Again, the authors measured a powerlaw distribution for sufficiently large avalanche sizes only, but not for small to intermediate avalanche sizes. Bak (1996, p.68) comments that the experiment records only those avalanches that fall off the plate, but ignores the avalanches that stop along the sandpile, because they do not introduce a change on the weight scale, and thus the distribution is incomplete.

An experimental setup with a inclined Plexiglas box, similar to the rotating drum of the Chicago group, was used by Bretz et al. (1992), but the avalanches of dry, noncohesive

granular material were recorded with a video camera. Again, the authors found a powerlaw distribution for small avalanches only, and Bak (1996, p.69) thought that the system they used was too small and the experiment was interrupted.

The ultimate and most careful experiment was performed by Frette et al. (1996) at the University of Oslo, who used rice piles instead of sand. Two-dimensional rice piles confined between two glass plates were monitored with video cameras to record the motion and size of individual rice grain avalanches, while additional rice grains were slowly added at the top of the pile. The experiment was performed for different plate distances, different system sizes (from a few cm to a few m), and for different rice types. The experimenters found that the occurrence distribution of energy (measured by the gravitational potential of the height difference between the beginning and end of an avalanche) dissipated in the rice avalanches obeyed a powerlaw function over up to 1.5 orders of magnitude, as expected for SOC behavior. However, the researchers found that the SOC behavior worked better for one type of rice (for grains with a large aspect ratio) than for others (for less elongated grains), and thus concluded that SOC is not universal, but depends on the detailed mechanism of energy dissipation. Note that this experiment records a complete sample of avalanches that stop on the pile or reach the end of the pile. A snapshot of the rice pile is shown in Fig. 1.3 (top left), the recorded area of a rice avalanche is displayed in Fig. 1.3 (top right)), and the frequency distribution of avalanche energies E, normalized by the system size L, is shown in Fig. 1.3 (bottom), which exhibits a powerlaw slope of $\alpha \approx 2.04$.

On a larger scale, if you combine a number of sandpiles, you end up with an entire landscape. Somfai et al. (1994a,b) at the Eötvös University in Budapest (Hungary) built their own mini-landscape in a laboratory and mimicked the landscape formation in nature by subjecting it to artificial erosion. A ridge-like landscape made of silica and potsoil was sprayed with water sprinklers, which produced mudslides of various sizes. They recorded the distribution of spatial sizes of mudslides and found a powerlaw with an exponent of $\alpha = 0.78 \pm 0.05$, which can be interpreted as evidence for SOC behavior. The resulting landscape was found to exhibit a fractal dimension, similar to that found in Norwegian fjords.

SOC behavior was also found in a number of laboratory experiments and in physical sciences, such as in plasma physics and material physics. A selection of phenomena that exhibit SOC behavior or to which SOC models have been applied is listed in Table 1.1 (adapted from Turcotte (1999)).

1.3 SOC in Human Activities

The unpredictability of outcomes in nonlinear dissipative systems is an inherent property of randomness, which is also called a Poisson process (see Chapter 4). The randomness occurring in our daily human life is one of the basic experiences that everybody accepts as a natural fact. A few examples of such Poisson processes in human life are: the number of cars that pass through a certain point on a road (sufficiently distant from traffic lights) during a given period of time; the number of spelling mistakes one makes while typing a single page; the number of phone calls at a call center per minute; the number of times a web server is accessed per minute; the number of light bulbs that burn out in a certain

Table 1.1 SOC behavior in material physics and laboratory plasma physics.

Phenomenon	References
sandpiles	Bak et al. (1989)
	Jaeger et al. (1989)
	Held et al (1990)
	Bretz et al. (1992)
rice piles	Frette et al. (1996)
silica and potsoil landscape	Somfai et al. (1994a,b)
fracture of fibrous materials	Bernardes and Moreira (1995)
microfracturing	Petri et al. (1994)
friction	Ciliberto and Laroche (1994)
random directed polymers	Jogi and Sornette (1998)
ceramics (Andrade creeps)	Cottrell (1996)
autocatalytic surface reactions	Drossel and Schwabl (1995)
annealed disorders	Caldarelli et al. (1996)
foam rheology	Okuzono and Kawasaki (1995)
	Kawasaki and Okuzono (1996)
dislocation networks	Marchesoni and Patriarca (1994)
lattice models of oscillators	Corral et al. (1995)
	Mousseau (1996)
pinned flux lattices	Pla and Nori (1991)
interface dynamics	Sneppen and Jensen (1993)
magnetic domain patterns	Babcock and Westervelt (1990)
	Che and Suhl (1990)
DC glow discharge plasma	Nurujjaman and Sekar-Iyenbgar (2007)
Barkhausen effect	Cote and Meisel (1991)
	O'Brien and Weissman (1994)
vortices in superconductors	Field et al. (1995)
	Zieve et al. (1996)
	Olson et al. (1997)
	Bassler and Paczuski (1998)
	Prozorov and Giller (1999)
plasma confinement	Carreras et al. (1996)
	Medvedev et al. (1996)
transport in tokamak plasmas	Kishimoto et al. (1996)
turbulence in tokamak plasmas	Rhodes et al. (1999)

amount of time; the number of roadkill (animals killed) found per unit length of road; the inventivity of inventors over their career; or the number of publications written by a scientist. Going back in time, the randonmness was even noted in the number of soldiers killed by horse-kicks each year in each corps in the Prussian cavalry, an example that was made famous in the book *The Law of Small Numbers* by Ladislaus Josephovich Bortkiewicz (1898).

Exploring the randomness in nature we will find Poisson processes everywhere: such as in the number of stars in a given volume of space, in the number of pine trees per unit area of mixed forest, in the number of viruses that can infect a cell in cell culture, in the number of hematopoietic stem cells in a sample of unfractionated bone marrow cells, in the distribution of visual receptor cells in the retina of the human eye, in the number of

mutations in a given stretch of DNA after a certain amount of radiation, in the number of unstable nuclei that decay within a given period of time in a piece of radioactive substance, or in the number of particles that scatter off a target in a nuclear or high energy physics experiment.

Since we can easily gather statistics on event sizes that occur in such random processes, we can test whether the statistical distributions match the mathematical powerlaw distributions that are expected in the state of self-organized criticality (Chapter 3). Such occurrence distributions, where the number N of events is statistically sampled versus the size S of the event, preferentially on a log-log scale, i.e., log(N) vs. log(S), so that the powerlaw function appears as a straight line, have been sampled for city sizes, word counts in English literature (Zipf's law; Saichev et al. 2009), cotton prices, stock-market, lottery wins, or traffic jams, as they are eloquently described in Bak's book, *How Nature Works*. We will look at some of these examples in more detail in the following.

Let us consider the sizes of settlements, villages, towns, and cities on a continent. There are obviously a lot of small towns, while there are only a few large cities, such as New York or Los Angeles. If we look at a geographical map of North America (Fig. 1.4, left panel), there are millions of settlements and villages with small communities, which aggregated apparently randomly at almost any livable place, near rivers (to have water support), near roads (to have access to traffic), or near coasts (to take advantage of ocean transportation). So, people gathered in small communities for some economic or survival benefit. In some places, economic growth was more favorable than in others, which attracted more people who left a poor countryside and moved to small towns where lifestyle was more promising. Improvement of lifestyle and economic growth caused more urban sprawl so that large cities grew, up to the limit of the *carrying capacity*. Thus the size of a community is the result of complex human interactions between many members, which can be considered as a *nonlinear dissipative system*. So, we expect a powerlaw distribution of city sizes, if urban growth is in the state of *self-organized criticality*. First statistics of city sizes was already

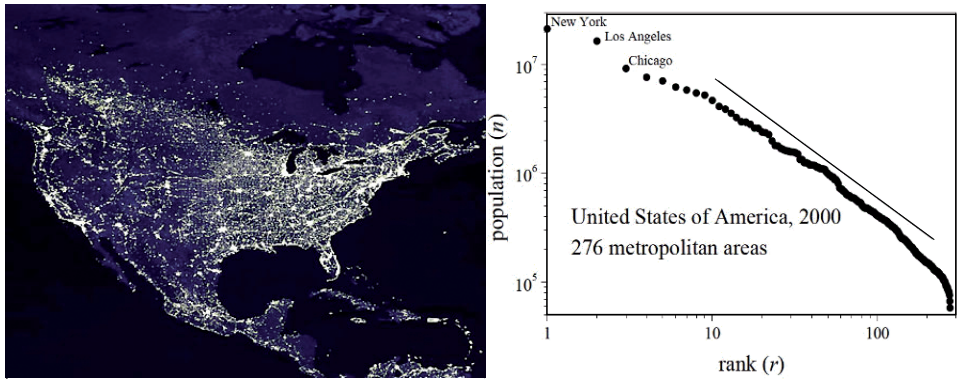

Fig. 1.4 *Left:* Satellite picture of North America at night, taken from the orbiting International Space Station (courtesy of NASA). The sizes of the light dots scale with the sizes of cities. *Right:* Zipf rank plot for 276 metropolitan areas in the United States, after results of the census in 2000. Source: http://factfinder.census.gov (Zanette 2007).

gathered by George Kingsley Zipf in 1920, when he produced a log-log histogram of the number of inhabitants per city versus the rank number of cities (which is essentially the order in a cumulative distribution), published in the book *Human Behavior and the Principle of Least Effort* (Zipf 1949). There were only a few cities larger than 8 million, 10 cities larger than 1 million, and 100 larger than 200,000. So, he found a powerlaw distribution with a slope of about $\log(N_2/N_1)/\log(S_2/S_1) \approx \log(100/10)/\log(2\times10^5/10^6) \approx -1.4$ for the cumulative occurrence distribution. A modern version of Zipf's plot is shown in Fig. 1.4 (right panel), based on a census in 2000 on 276 metropolitan areas in the United States
indexcensus (Zanette 2007). An up-to-date tutorial review on multiplicative processes in urban growth that lead to Zipf's law of city sizes is given in the same paper by Zanette (2007). Zipf's law applies also to the distribution of family names, or the number of individuals that speak the same language, because they are subject to the same multiplicative growth or inheritance process that is common to all biological systems.

Zipf (1949) also investigated the complexity of a language. In particular, he counted how often each word is used in a text of English literature, such as in James Joyce's *Ulysses* or in a collection of American newspapers. The most frequently used words in English texts are, in order of frequency, *"the", "of", "and", "in", "to", "a", "is", "that", "it", "as", "this", "by", "for", "be", "not"*, etc. If one plots the number of these words versus their rank, similarly to the Zipf plots of city ranks, one finds invariably a powerlaw distribution with a slope of ≈ -1. Computer programs that can be downloaded from the web (e.g., http://www.hermetic.ch/index.php) allow the user to produce such a Zipf plot for any arbitrary text. What is the reason for this powerlaw or SOC behavior? The use of every word is the result of complex thinking processes in our brain that involve associations of word concepts with perceived objects and logical connections that are expressed in verbal sentences. Associations or connections have a multiplicative functionality, and thus the word frequency or usage is proportional to the number of (meaningful) connections. Multiplicative behavior is an inherent characteristics of nonlinear systems, and thus enables SOC behavior. So, building up a complex language with rules of semantics, we end up with a word frequency that depends on the number of possible (i.e., meaningful) combinations, which is somehow multiplicative, based on the generality and applicability of a word. Some words that describe very rare applications, e.g., abacinate (to blind by putting a hot copper basin near someone's eyes), abcedarian (a person who teaches the alphabet), abderian (given to incessant or idiotic laughter), etc., as you can find in a grandiloquent dictionary (http://www.islandnet.com/~egbird/dict/dict.htm), are obviously at the bottom of a Zipf rank plot, because the people who have heard of these words and even use them is the smaller the more specific the word content is. So, ultimately, the word usage is the result of an avalanche-like chain-reaction in communication, similar to the nonlinear-growth interactions in sand avalanches. Other applications of Zipf's Law to economics, especially the births and deaths of firms, can be found in the textbook of Saichev, Malevergne, and Sornette (2009).

SOC behavior was also found in economy (financial market, lottery wins, random drawings), which is governed by random input and nonlinear system dynamics. Mandelbrot (1963) collected data of monthly cotton prices over several years and plotted a log-log histogram of the monthly cotton price fluctuations, finding a Lévy distribution with a pow-

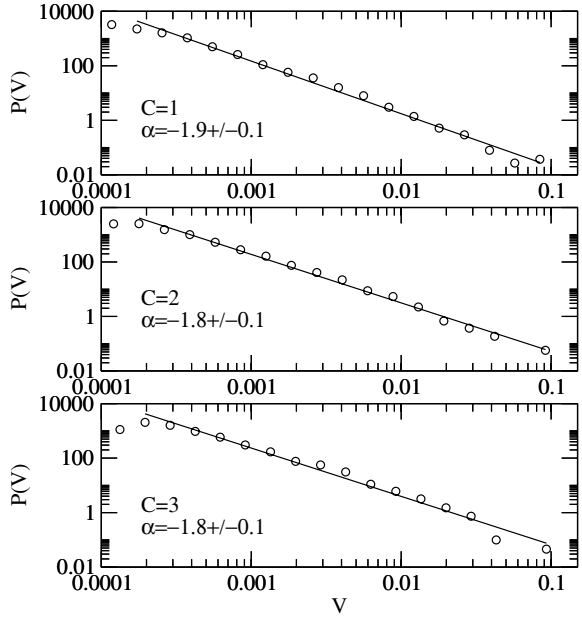

Fig. 1.5 Probability distribution function of "returns" (avalanche sizes) for the Dow Jones index daily closures from 1939/2/2 to 2004/4/13, computed for different cutoff parameters (in the selection of time intervals of high activity) using a wavelet method with three different settings (C = 1,2,3) (Bartolozzi et al. 2005).

erlaw tail with a slope of ≈ -1.0. More recently, fluctuations of the stock market have been investigated in great detail, which often show marginal variations of the daily Dow-Jones index, but occasionally can escalate into catastrophic events, such as the Wall Street crash in October 1929, the October 1987 market crash, or the big world-wide economic crisis in 2008 (at the time of writing). Stock market crashes, which can be triggered by speculation or political events, represent large avalanches in a SOC system (Scheinkman and Woodford 1994; Mantegna and Stanley 1997). The multiplicative chain reaction inherent to SOC systems has been modeled in terms of interacting producers and vendors by Bak et al. (1993, 1997). The avalanche-like evolution of stock market crashes is believed to be preceded by precursors with log-periodic fluctuations (Feigenbaum and Freund 1996; Sornette et al. 1996; Sornette and Johansen 1997). Recent studies (Bartolozzi et al. 2005) of the Nasdaq100, the (Standard and Poor's) S&P ASX50, and the Dow Jones index revealed powerlaws and SOC behavior for the logarithmic returns of these indices (avalanche sizes, see Fig. 1.5), the high activity periods (avalanche durations), and the quiet "laminar" times (waiting times). A recent progress report on financial physics reviews the application of SOC to economics, the Cont-Bourchaud percolation model, multiple-strategy agent-based models of financial markets, the minority game (i.e., the El Farol problem), and log-periodic precursors to financial crashes (Feigenbaum 2003).

A traffic jam is another driven dynamic system with random input that exhibits SOC behavior. Cars enter a highway at random times. If the traffic rate is low, such as on a

Sunday morning, the system is subcritical because there is plenty of space between subsequent cars so that they do not bother each other. During a rush hour, however, everybody is slowed down by the cars in front, and the spacings between subsequent cars is irregular due to different driving speeds, braking manoeuvres, car passings, delays in human reaction, or interfering weather conditions, etc. The distribution of car spacings will exhibit SOC behavior for a busy traffic situation with maximum throughput. If there is too high a traffic rate, the traffic slows down to a bumper-to-bumper situation. In fact, SOC is the most efficient state of traffic, because too low a rate is a waste in terms of under-utilized streets, while too high a rate leads to a permanent jam (Bak 1996). Emergent traffic jams were simulated by Nagel and Paczuski (1995), who found a powerlaw distribution of $N(t) \propto t^{-3/2}$ for the lifetimes of jams and $1/f$-noise in the power spectrum. Further models for traffic jams were studied by Nagel and Herrmann (1993), and Nagatani (1995a,b,c,d).

Other human activities, where a large number of individuals are involved and where random factors govern, are wars. The size or intensity of wars was quantified with the number of battle deaths and the statistical distribution of the number of wars versus the number of casualties was found to be a powerlaw distribution (Richardson 1941, 1960; Levy 1983; Roberts and Turcotte 1998; Turcotte 1999). But why are wars examples of SOC behavior? Turcotte (1999) compared the spread of wars over contiguous areas with people of identical political ideology and to metastable neighbor countries with the forest fire model, where a fire spreads over a contiguous local group of trees, and subsequently to neighboring tree groups, if they are located within a critical distance. The higher the number of trees per area, the larger is the size of the forest fire, similarly to how a local war can spread to a global conflict in case of high population density. However, while some statistical features of human activities can be modeled with a SOC model, we have to be aware that human interactions are far more complex (and arbitrary) than what can be modeled with a lattice model (Chapter 2) with well-defined probabilities.

A selection of references studying SOC behavior in human activities is summarized in Table 1.2.

1.4 SOC in Biophysics

Charles Darwin's theory of evolution explains life on Earth as a chain reaction of mutations, adaptation, survival of the fittest species, and elimination of the least-fit, resulting into a natural selection of the surviving species. Mutations of cells happen relatively rarely, for instance by absorption of ultraviolet light, with a higher probability for long-lived cells (which is the reason for a higher likelihood of cancer development in aging people). Since mutation happens rarely and in episodic steps, rather than with slowly-varying continuity, evolutionary changes occur in episodic bursts, separated by calm periods (similar to the stock market behavior). Evolutionary changes can include creation of new species as well as extinction of old species (like gains and losses on the stock market). The suggestion that evolution takes place in bursts separated by calm periods was made by Gould and Eldredge (1977). Statistics on the extinction of species were clearly found to be episodic at all times (Raup 1986; Sepkoski 1993, see Fig. 1.6), such as the famous Cretaceous-Tertiary event (65 million years ago) when dinosaurs became extinct, which was speculated to be

Table 1.2 SOC behavior in human activities.

Phenomenon	References
urban growth, city sizes	Zipf (1949)
	Zanette (2007)
word frequency in language	Zipf (1949)
cotton prices	Mandelbrot (1963)
stock market	Scheinkman and Woodford (1994)
	Feigenbaum and Freund (1996)
	Sornette et al. (1996)
	Sornette and Johansen (1997)
	Mantegna and Stanley (1997)
	Feigenbaum (2003)
	Bartolozzi et al. (2005)
traffic jam	Bak (1996)
	Nagel and Herrmann (1993)
	Nagel and Paczuski (1995)
	Nagatani (1995a,b,c,d)
war casualties	Richardson (1941, 1960)
	Levy (1983)
	Roberts and Turcotte (1998)
social networks	Newman et al. (2002)
internet traffic	Willinger et al. (2002)

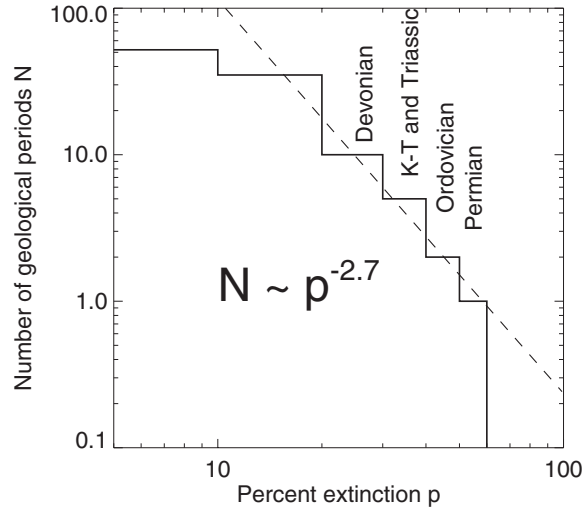

Fig. 1.6 Log-log histogram of the number of biological extinction events over the last 600 million years as recorded by Sepkoski Jr., who estimated from fossil records the percent of families that went extinct within time periods of approximately 4 million years. The dashed line shows a powerlaw fit of $N \propto p_{ext}^{-2.7}$ (adapted from Sepkoski 1993).

a consequence of an asteroid impacting Earth. An even bigger extinction event happened during the Cambrian era (500 million years ago), when up to 95% of all species on Earth disappeared. Raup (1991) discusses the origins of extinctions in his book *"Extinction: Bad Genes or Bad Luck?"* An extinction phase can involve a chain reaction of multiple species, which may depend on each other. On the other hand, the extinction of one species can trigger the growth of another competing species. Dinosaurs and mammals were believed to co-exist for a long period of time, while the number of mammal species grew explosively after the disappearance of dinosaurs, because their degree of fitness increased without the competition of the giant dinosaurs. Episodic changes in the size of species can also be triggered by meteorological changes. Warm-blooded mammals may die at higher rates during ice-ages. Global warming periods increase the overall temperature, which can enhance the probability for the spread of diseases, since chemical reactions generally occur at a rate of a factor of two faster when the temperature rises by 10%, speeding up the spread of pandemic diseases.

The episodic evolution and extinctions of species that leads to the biodiversity at a given time has been characterized with a model called *punctuated equilibria model* (Gould and Eldredge 1977, 1993). The dynamical concept consists of bursty episodes of high activity (i.e., punctuated events, like selected points in a time series), and calm intervening time intervals of low activity (i.e., waiting times; Chapter 5), where the dynamic system settles into a near-equilibrium state. A simple model of biological evolution based on punctuated equilibrium and criticality was developed by Bak and Sneppen (1993), which self-organizes into a critical steady state with intermittent co-evolutionary avalanches of all sizes. This concept involves "collaborative evolution", which is much more efficient than noncooperative scenarios with independent (and thus unlikely) mutation steps. The punctuated or stepwise behavior of evolutionary changes was reproduced by numerical simulations (Maslov et al. 1994). A unified class of systems far from equilibrium processes, including the Bak–Sneppen evolution model, interface depinning models, and invasion percolation models, was combined by Paczuski et al. (1996). A general discussion of criticality and scaling terms in evolutionary ecology is given in Sole et al. (1999). A more recent model on the time-dependent extinction rate and species abundance is the *tangled-nature model* (Hall et al. 2002), which reproduces both a smooth evolution of microscopic fluctuations as well as intermittency of macroscopic fluctuations (punctuated equilibria). Some other applications of SOC models to biophysics are given in Table 1.3.

1.5 SOC in Geophysics

An excellent introduction into the subject of self-organized criticality in Earth systems can be found in the textbook of Hergarten (2002), with extensive coverage on earthquakes, landslides, and drainage networks. Another textbook related to this subject covers fractals and chaos in geology and geophysics (Turcotte 1997). Besides seismology and earthquakes, SOC behavior is also found in a number of other geophysical systems, such as in landslides, turbidites, geological layers, volcanic eruptions, forest fires, lightning, rainfall, hydrology, snow avalanches, cloud formation, climate fluctuations, etc.; see Table 1.4 for a representative selection.

Table 1.3 SOC in biophysics.

Phenomenon	References
evolution and extinctions	Gould and Eldredge (1977) Raup (1986) Sepkoski (1993)
neuron firing in a brain	Stassinopoulos and Bak (1995) Hopfield (1994) Rundle et al. (2002)
neural reverberations of spiking nerve cells	Herz and Hopfield (1995) da Silva et al. (1998)
learning and memory	Chialvo and Bak (1999)
breathing in lung	Barabasi et al. (1996)
heart rate	Goldberger et al. (2002)
epileptic seizures	Osorio et al. (2009a,b)
spread of diseases	Johansen (1994)
measles epidemics	Rhodes and Anderson (1996) Rhodes et al. (1997)
flying formation of birds	Nathan and Barbosa (2006)
termite nest architecture	O'Toole et al. (1999)
phylogenetic (evolutionary) trees	Vandewalle and Ausloos (1995)

Table 1.4 SOC in geophysics.

Phenomenon	Selected references
earthquakes	Gutenberg and Richter (1954) Aki (1981) Bak et al. (2002)
landslides	Fuyii (1969) Hovius et al. (1997, 2000) Pelletier et al. (1997) Malamud et al. (2001)
turbidite depositions	Rothman et al. (1994)
volcanoclastic turbidite deposits	Hiscott et al. (1992)
volcanic acoustic emission	Diodati et al. (1991, 2000)
volcanic activities	Grasso and Bachelery (1995)
rock texture in craters	Wu and Zhang (1992)
plastic shear bands in rocks	Poliakov and Herrmann (1994)
epizonal mineral deposits	Henley and Berger (2000)
propagating brittle failure	Katz (1986)
snow avalanches	Birkeland and Landry (2002)
river networks	Rinaldo et al. (1996)
drainage networks	Hergarten (2002)
Nile river fluctuations	Hurst (1951)
rainfall	Andrade et al. (1998)
cloud formation	Nagel and Raschke (1992)
climate fluctuations	Grieger (1992)
aerosols in atmosphere	Kopnin et al. (2004)
forest fires	Kasischke and French (1995) Malamud et al. (1998)

Earthquakes represent local adjustments to the stressing forces in the upper earth crust (in depths of less than 20 km), which is not static but experiences permanent deformation. The lithosphere is subdivided into several tectonic plates, whose motion is driven by thermal convection in the mantle giving rise to spreading centers ocean ridges and subduction zones at ocean trenches. The tectonic plates behave elastically until the stresses exceed a certain threshold and a displacement occurs as a consequence – like a stick-and-slip motion – reducing the stress. Earthquakes can also strike in the stable crust, far away from earthquake zones at the edges of tectonic plates (Johnston and Kanter 1990) or hidden on "blind" faults under folded terrain (Stein and Yeats 1989). Earthquakes are episodic and intermittent events, separated by long time intervals of quiescence, sometimes preceded by precursors, or followed by aftershocks. Once an earthquake occurs, seismic waves propagate away from the epicenter and cause damage over an extended area. Statistics of earthquakes and measurements of their magnitude became a research focus during the 20th century. The Gutenberg and Richter (1954) law was established already more than a half century ago. It states that the cumulative distribution of earthquakes follows a powerlaw distribution as a function of the magnitude m. A similar relation holds for the earthquake rupture areas A_E, i.e., $N^{cum}(>A_E) \propto A_E^{-1}$, or $N(A_E) \propto A_E^{-2}$ for the differential occurrence frequency distribution (Aki 1981). [Definitions of differential and cumulative frequency distributions are provided in Section 7.1.] The world-wide statistics of earthquakes for the period of 1977–1994 is given in Fig. 1.7, as a function of the Gutenberg–Richter magnitude m (top axis), as well as a function of the earthquake rupture area A_E (bottom axis).

The relationship of earthquakes to self-organized criticality has been considered by Bak and Tang (1989), Sornette and Sornette (1989), Ito and Matsuzaki (1990), Sornette

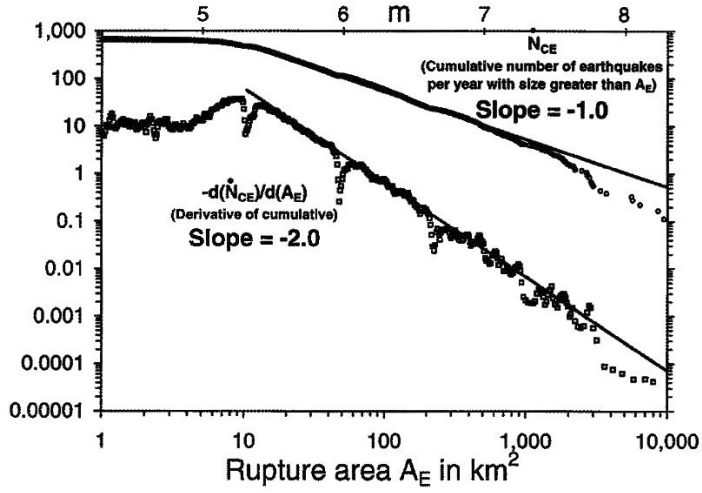

Fig. 1.7 World-wide cumulative (slope $= -1$) and differential frequency distribution (slope $= -2$) of earthquakes per year as a function of the rupture area A_E in units of square kilometers, based on the Harvard Centroid-Moment Tensor Data Base (1997) for the years 1997–1994. The conversion into equivalent Gutenberg–Richter magnitudes m is indicated on the top axis (Turcotte 1999).

et al. (1990), Olami et al. (1992), Bak and Chen (1995), and Huang et al. (1998). The fractal dimension of the distribution of earthquake fault gouges was brought into context with the powerlaw behavior of SOC (Sammis et al. 1987). The primary SOC models applied to earthquakes are the Burridge and Knopoff (1967) slider-block model (see reviews by Carlson et al. 1994, Turcotte 1997, 1999, and references therein), while other SOC models include crack propagation (Chen et al. 1991) and interface depinning (Paczuski and Böttcher 1996; Fisher et al. 1997). The waiting times between earthquakes were also found to obey a powerlaw distribution, within a validity range of tens of seconds to tens of years (Bak et al. 2002).

Major natural hazards on Earth include earthquakes, snow avalanches, floods, storms, volcanic eruptions, and landslides, which all exhibit SOC behavior (Hergarten 2002). Landslides occur mostly in mountainous areas (Fig. 1.8), where the inclination angle exceeds a critical slope, similar to the sand and rice piles discussed in Section 1.2. A more physical term for landslides is *gravity-driven mass movements*. Landslides can be triggered by heavy rainfall or earthquakes. After the initial detachment of a certain amount of soil, gravity will accelerate the unstable mass and increase the kinetic energy gradually. The increasing speed will overcome more friction at the front and edges of the sandslide and pull more material along, further increasing the mass and kinetic energy. Landslides and avalanches, therefore, exhibit a multiplicative or exponential-like growth in the time evolution of their area, volume, mass, and energy. Landslides were found to have multifractal properties (Mandelbrot 1985; Feder 1988; Turcotte 1997). Cumulative frequency distributions of landslides as a function of the area (or some other magnitude definition)

Fig. 1.8 A sketch of the mountain "Rossberg" in Arth/Goldau (Switzerland), where a catastrophic rockslide occurred on September 2, 1806 and destroyed the town of Goldau, causing the death of 457 people (drawing by Fritz Morach).

were found to exhibit a powerlaw distribution with slopes of $\beta = 0.96$ in Japan (Fuyii 1969), $\beta = 1.16$ in New Zealand (Hovius et al. 1997), $\beta = 0.70$ in Taiwan (Hovius et al. 2000), $\beta \approx 1.6$–2.0 in Japan, California, and Bolivia (Pelletier et al. 1997), or $\beta = 1.5$ in Italy (Malamud et al. 2001). This powerlaw slope range of $\beta \approx 0.7$–2.0 for cumulative frequency distributions corresponds to $\alpha = \beta + 1 \approx 1.7$–$3.0$ for differential (noncumulative) frequency distributions. Sandslides triggered by earthquakes revealed powerlaw slopes in the range of $\alpha = 2.3$–3.3 for datasets from California, Japan, and Bolivia (see review by Turcotte 1999 and references therein). Frequency distributions of sandslide volumes with powerlaw behavior have been measured over 12 orders of magnitude, on Himalayan roads (Noever 1993). The frequency distributions and fractal properties of landslides seem not to depend on the triggering event (earthquake or rainfall), nor on the steepness of the mountain slope (except for very shallow angles). Theoretical models of sandslides include the classical BTW sandpile model (Bak et al. 1989), the OFC spring-block model (Olami et al. 1992), or physics-based models, e.g., based on partial differential equations that combine the slope stability and mass movements (Hergarten and Neugebauer 1998).

Sediment depositions at the edge of the continental shelf, deposited some 100 million years ago, occurred also as avalanche-like events, called slumps. The resulting sediment layers are called turbidites and have a variety of sizes and thicknesses, which were found to exhibit a powerlaw distribution in the geological layer thicknesses, e.g., as measured in the Death Valley in California (Rothman et al. 1994). Similar powerlaw distributions that indicate SOC behavior have been found in volcanoclastic turbidite deposits (Hiscott et al. 1992), in acoustic emission from volcanic activity of Stromboli (Diodati et al. 1991, 2000), in rock textures and multi-ring structures in the Duolun crater (Wu and Zhang 1992), in plastic shear bands in rocks (Poliakov and Herrmann 1994), in epizonal mineral deposits (Henley and Berger 2000), in the eruptions, volcano-induced earthquakes, dikes, fissures, lava flows, and interflow periods of the *Piton de la Fournaise* volcano (Grasso and Bachelery 1995), in dust grains (aerosols) in the Earth's atmosphere (Kopnin et al. 2004), or in snow avalanches (Birkeland and Landry 2002).

Water plays a fundamental role for life on earth. All parts of the water cycle, from evaporation over the oceans, to formation of clouds, to rainfall, to river formation, were also found to exhibit SOC behavior. Water-related phenomena are studied in the sciences of hydrology and rheology. The formation of small water streams that combine to bigger and bigger rivers exhibit a well-known fractal pattern, also known as Horton's law. Horton's law defines the order of river segments as the number of links to other segments that have to be passed before the river reaches the ocean, which increase as a powerlaw in the order. The most famous manifestation of this principle is the fractal coastline of Norway. River networks and drainage networks have been studied systematically under the aspect of SOC (e.g., Rinaldo et al. 1996; Hergarten 2002). The fluctuations of the water level of the Nile river has been characterized with a Hurst exponent (Hurst 1951), which is related to SOC behavior. SOC behavior was also studied in rainfall (Andrade et al. 1998), cloud formation (Nagel and Raschke 1992), and climate fluctuations (Grieger 1992), which are now in hot debate in the context of the global warming trend.

Forest fires are another phenomenon that exhibit classical SOC behavior. The trigger may be a small accident, such as an out-of-control campfire, a discarded cigarette, or an electric spark of a high-voltage power line, while the outcome can have catastrophic di-

mensions, depending on the spreading efficiency that can be sped up by dry conditions or wind. The noncumulative frequency distribution of the number of forest fires as a function of burned area was found to have a powerlaw slope of $\alpha = 1.3$ for 4284 fires on US Fish and Wildlife Service land during 1986–1995 (National Interagency Fire Center), $\alpha = 1.3$ for 120 fires in the western US during 1955–1960, calculated from tree ring data (Heyerdahl et al. 1994), $\alpha = 1.4$ for 164 fires in Alaskan Boreal Forests during 1990–1991 (Kasischke and French 1995), or $\alpha = 1.5$ for 298 fires in the Australian Capital Territory during 1926–1991 (ACT Bush Fire Council 1996), as computed by Malamud et al. (1998). Forest fires were one of the first phenomena that have been modeled with a SOC cellular automaton model (Bak et al. 1990; Drossel and Schwabl 1992a,b; Henley 1993). More comprehensive forest-fire models were developed that include also phase transitions, "immune" trees, and applications of the renormalization group theory (see review by Turcotte (1999)).

1.6 SOC in Magnetospheric Physics

Magnetospheric physics deals with the interaction of the Earth's (or some other planet's) magnetic field with the ambient solar wind in the heliosphere, which triggers a host of secondary phenomena, such as ionospheric electric currents, aurorae, magnetic storms, substorms, magnetic reconnection, and turbulence. Some dynamic phenomena occur in the plasma sheet and neutral sheet of the geotail, in the trailing part of the Earth's magnetic field that stretches out past 200 Earth radii away from the Sun. A lot of magnetospheric events (storms) are triggered by solar flares, coronal mass ejections, and the solar wind, which have a highly intermittent and turbulent dynamics, but mostly exhibit SOC behavior. Magnetospheric substorms and auroral activity evolve in response to the solar wind and exhibit distinctly different levels of activity and nonequilibrium phase transitions (Bargatze et al. 1985; Sitnov et al. 2000). Therefore, the bursty nature of magnetospheric phenomena, such as localized current disruptions (Lui et al. 1988), bursty bulk flow events (Angelopoulos et al. 1996, 1999), and the powerlaw magnetic field spectra in the magnetotail (Hoshino et al. 1994), have been interpreted in terms of an open, dissipative nonlinear system near a forced or self-organized critical state (Chang 1992, 1999a,b; Klimas et al. 2000; Chang et al. 2003; Chapman and Watkins 2001; Consolini and Chang 2001). Evidence for the powerlaw characteristics of the probability distribution of energy release events was found in auroral images from Polar/UVI (Lui et al. 2000; Uritsky et al. 2002, 2003, 2006), in ground-based optical auroral observations (Kozelov et al. 2004), in the burst size of the *auroral electron jet index (AE)* (Takalo et al. 1993; Consolini 1997, 2002), or in magnetospheric substorm-related tail current disruptions (Consolini and Lui 1999). An example of an auroral image is shown in Fig. 1.9, and statistics of auroral blob sizes are shown in Fig. 1.10, where a powerlaw distribution over two orders of magnitude is observed for auroral blob areas during quiet time intervals, but not during substorms.

Physical models of the dynamics of the Earth's magnetotail are described in terms of stochastic behavior of a nonlinear dynamical system near forced and/or self-organized criticality. Multi-scale intermittent turbulence of overlapping plasma resonances and current-driven instabilities are believed to lead to the onset and evolution of substorms, which

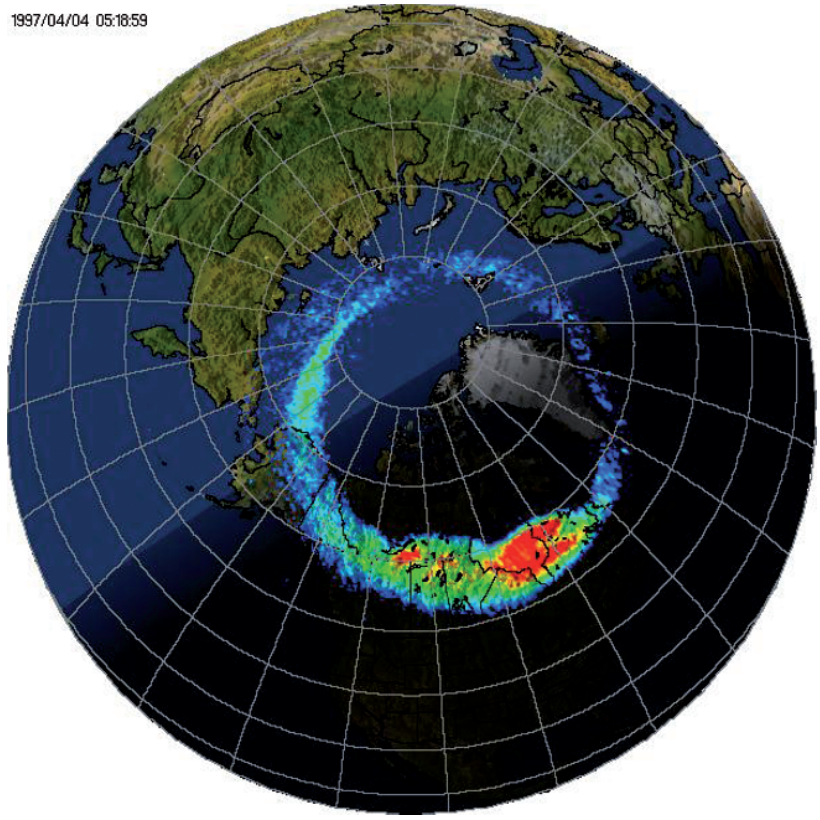

Fig. 1.9 Global image of the auroral oval observed by the Ultraviolet Imager (UVI) onboard the NASA satellite "Polar" on April 4, 1997 at 0519 UT, projected onto an Earth map (credit: NASA, Polar/UVI Team, George Parks).

Table 1.5 SOC in magnetospheric physics.

Phenomenon	Selected references
magnetotail current disruptions	Lui et al. (1988)
substorm current disruptions	Consolini and Lui (1999)
bursty bulk flow events	Angelopoulos et al. (1996, 1999)
magnetotail magnetic field	Hoshino et al. (1994)
auroral UV images	Lui et al. (2000) Uritsky et al. (2002, 2003, 2006)
auroral optical images	Kozelov et al. (2004)
auroral electron jet index (AE)	Takalo et al. (1993) Consolini (1997, 2002)

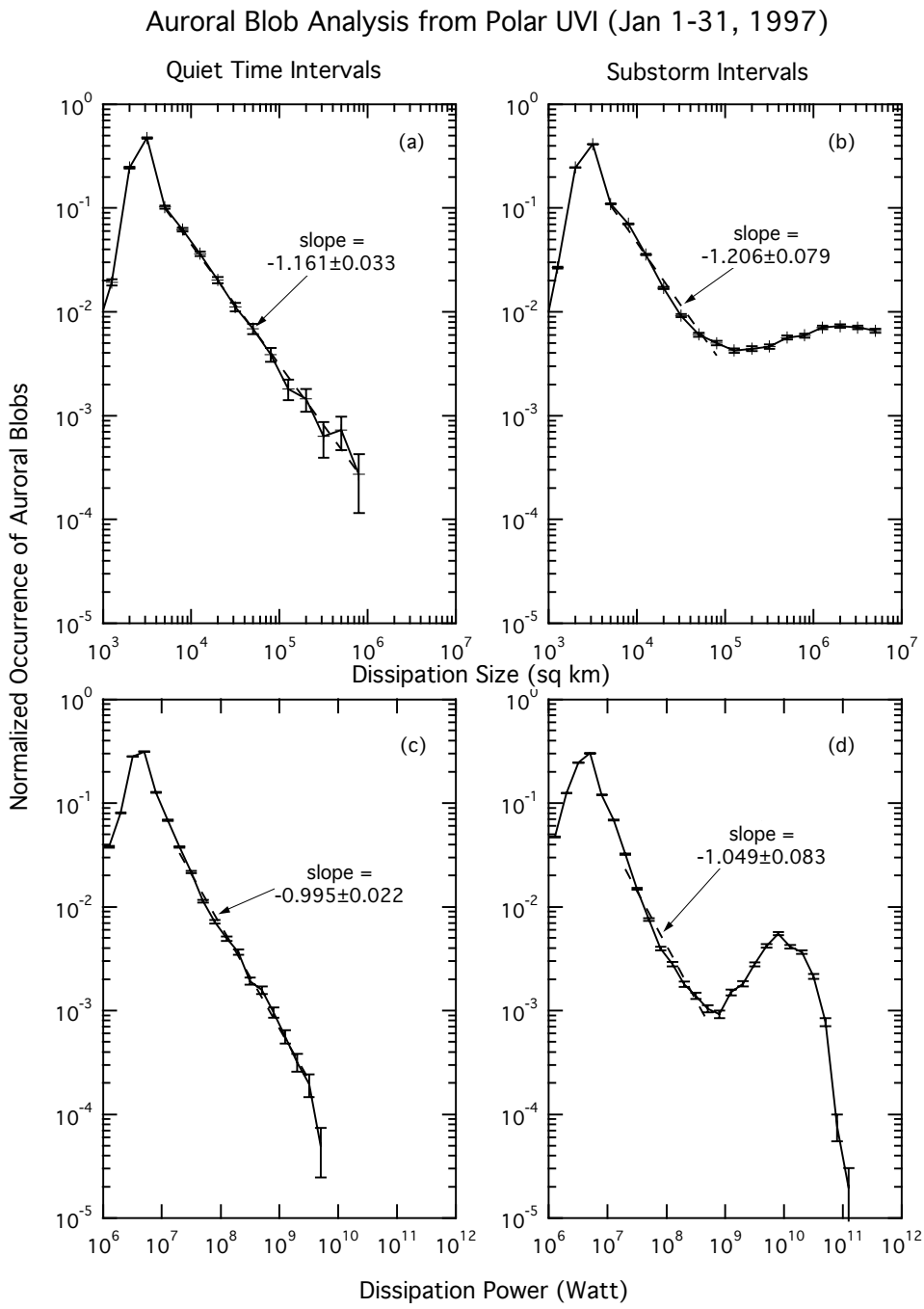

Fig. 1.10 Occurrence rate frequency distributions of auroral blobs (see Fig. 1.9) as a function of the size (top panels) or dissipated energy (bottom panels), during quiet time intervals (left panels) and active time intervals (right panels) (Lui et al. 2000).

explains the localized and sporadic nature of bursty magnetic reconnection and the fractal spectra observed in the magnetotail region (Chang 1999a,b; Klimas et al. 2000, 2004). Extending the original definition of SOC by Bak et al. (1987), Chang (1992) introduced the term *forced criticality*, which differs from Bak's SOC model in the sense that it is critical without self-organization, under the influence of external forcing. Coherent magnetic structures approach each other and merge or scatter under the influence of external forcing, turbulence, or self-organization, until a powerlaw-like spectrum of size scales occurs. It is now argued that the magnetospheric system is driven to a critical or near-critical state as a result of the continuous loading and subsequent unloading above a critical current (Chang 1992, 1999a,b; Consolini and de Michelis 2002; Horton and Doxas 1996). The new model eliminates the older "dripping faucet" model of chaotic loading and unloading (Baker et al. 1990; Klimas et al. 1992). Various cellular automaton SOC models have been developed to model the dynamics of the auroral electron jet (AE) index (Uritsky and Pudovkin 1998; Chapman et al. 1998, 1999; Watkins et al. 1999), the magnetotail current sheet (Takalo et al. 1999a,b; Milovanov et al. 2001), the central plasma sheet (Liu et al. 2006), and extended with renormalization-group analysis (Tam et al. 2000). Some observational references for magnetospheric SOC phenomena are given in Table 1.5.

1.7 SOC in Planetary Physics

A number of SOC phenomena studied in geophysics (earthquakes, volcanic eruptions, landslides, meteorite impacts) are expected to occur also on other rock-like planets, moons, or asteroids. Even water-related phenomena (river networks, fluvial systems, sedimentation) are expected on planets that carried water at some time (e.g., Mars). Planets with atmospheres (Venus, Mars, Jupiter, Saturn, Uranus, Neptune, etc.) are expected to exhibit SOC behavior in climate phenomena (e.g., dust storms, climate changes, transient spots and eddies, latitudinal bands). Planets with magnetic fields (Mercury, Jupiter, Saturn, Uranus, Neptune) are expected to show SOC behavior in magnetospheric phenomena (aurorae, substorms). However, due to the remote location and limited spatial resolution of Earth-bound observations we have very little data on planetary SOC phenomena.

Mars global dust storms do not occur every year, but preferably during late southern spring, when Mars is near its perihelion closest to the Sun. This interannual variability of Mars global dust storms was modeled in terms of a SOC system, where smaller storms ("dust devils") occur between the active years at a lower threshold (Pankine and Ingersoll 2004). SOC models were also applied to the Martian fluvial system (Rosenshein 2003). Self-organized criticality produces avalanches that grow coherently by nearest-neighbor interactions, generally forming size distributions that obey a powerlaw function. In a wider sense, we can even consider accretion, collisions, and scattering of particles as nonlinear dissipative processes possibly governed by SOC behavior. Such nonlinear processes are expected in the formation of planetary systems, planetary rings, asteroids, comets, meteorites, and circumplanetary dust. The distribution of particle sizes in Saturn's ring (Fig. 1.11) indeed follows a powerlaw distribution of $N(L) \propto L^{-3}$ in the range of $1\,\mathrm{mm} < L < 20\,\mathrm{m}$ (Zebker et al. 1985; French and Nicholson 2000). The asteroid size distribution follows a broken powerlaw with $N(L) \propto L^{-2.3}$ for large asteroids (5–50 km) and

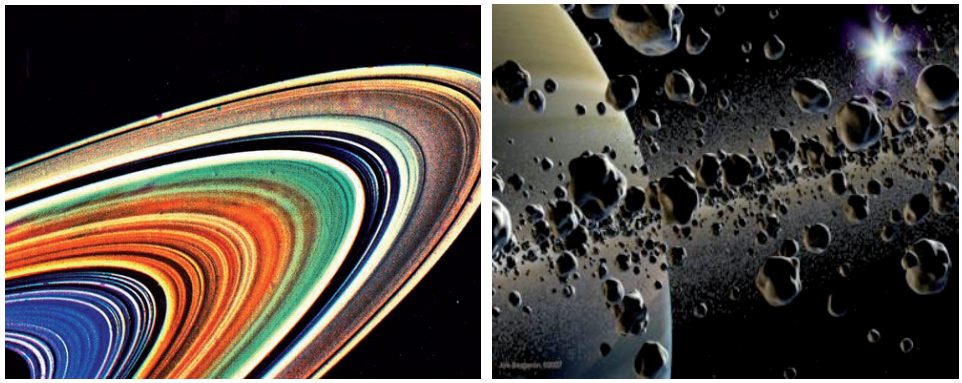

Fig. 1.11 Saturns rings observed by Voyager 2 spacecraft (left panel, credit: JPL and NASA), and artistic rendering of saturn ring particles in close-up (right panel).

$N(L) \propto L^{-4}$ for smaller asteroids (0.5–5 km) (Ivezic et al. 2001). The size distribution of lunar craters was found to be approximately $N^{cum}(>L) \propto L^{-2}$ (Cross 1966).

1.8 SOC in Solar Physics

Solar flares are very energetic phenomena where a magnetic reconnection process liberates large amounts of magnetic energy that is dissipated by heating of thermal plasma and by acceleration of high-energy (nonthermal) particles. The high-energy particles propagate along the coronal magnetic field lines and mostly slam into the dense plasma in the chromosphere, while a small fraction escapes upward into interplanetary space. The majority of accelerated particles that precipitate into the chromosphere produce collisional bremsstrahlung in hard X-ray and gamma ray wavelengths, while heated chromospheric plasma "evaporates" up into the postflare loops (Fig 1.12). The hard X-ray emission, which provides a good measure for the total released flare energy, has been recorded for a large number of flares with the *Solar Maximum Mission (SMM)* spacecraft during 1980–1989. When a frequency distribution of these many hard X-ray peak count rates was plotted, an astonishingly straight powerlaw distribution with a slope of $\alpha \approx 1.8$ was found (Dennis 1985), extending over 4 orders of magnitude (Fig. 1.13). Statistics of other flare parameters were calculated, yielding a powerlaw slope of $\alpha = 1.73 \pm 0.01$ for background-subtracted hard X-ray peak rates, $\alpha = 2.54 \pm 0.05$ for flare durations, and $\alpha = 1.53 \pm 0.03$ for nonthermal electron energies above 25 keV (Crosby et al. 1993).

Powerlaw distributions of flare peak intensities were found in virtually all observed wavelengths: in gamma rays, hard X-rays, soft X-rays, extreme ultraviolet, Hα, optical, and radio wavelengths (see Table 1.6 for observational references). Although the values of the powerlaw slope varies over a considerable range ($\alpha \approx 1.1$–2.8) in different wavelengths, most measurements fall in the range of $\alpha \approx 1.5$–1.9. With the advent of hard X-ray detectors with higher sensitivity, the frequency distributions were considerably extended at the lower end, to flares that were smaller up to 3 orders of magnitude, called *microflares*

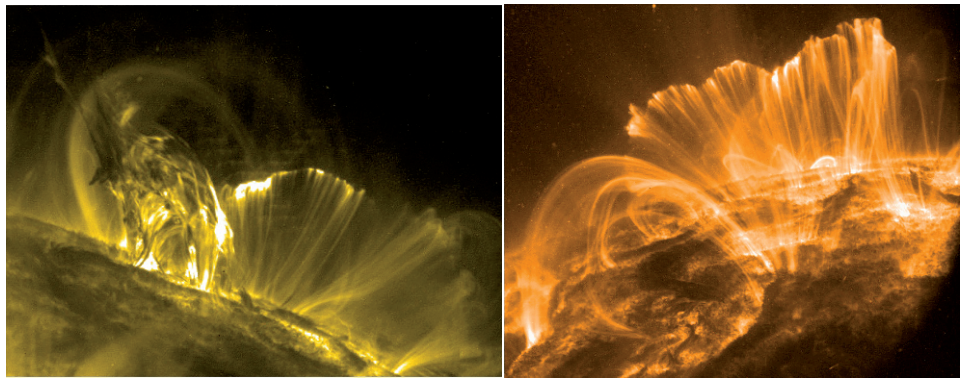

Fig. 1.12 Solar flares observed in EUV with the TRACE spacecraft in 171 Å: The flare of 2001 Apr 15 exhibits an erupting filament in the foreground and a rising postflare arcade behind near the limb (left panel), while the 2000 Nov 9 flare displays the 3-D geometry of the double-ribbon postflare arcade (right panel) (credit: NASA, TRACE).

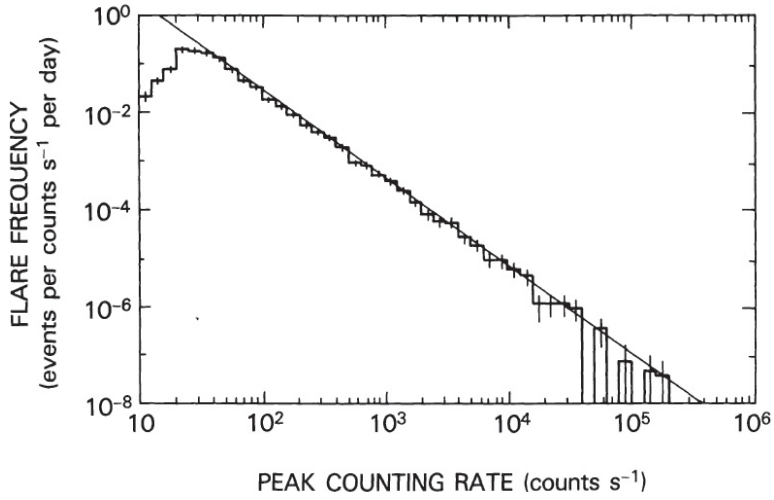

Fig. 1.13 Occurrence frequency distribution of the peak count rate of over 6,000 hard X-ray flares with photon energies above 25 keV, recorded with the *Hard X-Ray Burst Spectrometer (HXRBS)* onboard NASA's *Solar Maximum Mission (SMM)* during 1980–1985. The distribution follows a powerlaw with a slope of $\alpha \approx 1.8$ over 4 orders of magnitude (Dennis 1985).

(e.g., Lin et al. 2001; Christe et al. 2008). A further extension down to 9 orders of magnitude smaller than the largest flares could be observed with high-resolution EUV imagers (SOHO/EIT, TRACE), called *nanoflares* (e.g., Krucker and Benz 1998; Aschwanden and Parnell 2002). Because the powerlaw slope of the frequency distributions was found to be close to $\alpha = 2$ for nanoflares, which is a critical limit where the energy integral diverges at the low or high end, the crucial question came up whether nanoflares significantly con-

tribute to coronal heating (Hudson 1991). A synthesized frequency distribution of flares, microflares, and nanoflares is shown in Fig. 1.14, which exhibits an approximate powerlaw distribution with an overall slope of $\alpha \approx 1.8$ for the flare peak fluxes. Flares with or without coronal mass ejections (CME) were found to have different powerlaw slopes (Yashiro et al. 2006). The exact value of the powerlaw slope depends on event selection, event definition, instrumental sensitivity or flux threshold, instrumental bias, observed wavelengths and temperature regime, geometric models, and energy definitions (e.g., Lee et al. 1995; Isliker and Benz 2001; Aschwanden and Charbonneau 2002; Aschwanden and Parnell 2002; McIntosh and Charbonneau 2001; McIntosh et al. 2002). Another question was how robust the flare frequency distribution is in time. No significant variation of the powerlaw slope was found during the 11-year solar cycle (Bai 1993), although the flare rate varies by orders of magnitude. The flare frequency distributions were also investigated as a function of the spatial size of the associated active regions and some dependencies of the powerlaw slopes and cutoffs were found (Wheatland and Sturrock 1996; Kucera et al. 1997; Sammis 1999; Wheatland 2000c).

While most of the flare emission in hard X-rays, soft X-rays, and EUV is confined to the lower corona, flare-associated phenomena in the upper corona or heliosphere include coronal mass ejections (CMEs), radio bursts, shock waves, and solar energetic particle (SEP) events. Powerlaw distributions of these secondary events in the flare process have been observed for radio bursts and solar energetic particles (see Table 1.6). For CMEs there are probably no suitable data available, because measured observables are the angular width and propagation speed, while CME masses or energies require model-dependent calculations that are not readily available.

An interpretation of the omnipresent powerlaw distributions of flare peak fluxes or energies in terms of SOC models was first proposed by Lu and Hamilton (1991), from which we quote the abstract: *"The solar coronal magnetic field is proposed to be in a self-organized critical state, thus explaining the observed powerlaw dependence of solar-flare-occurrence rate on flare size which extends over more than five orders of magnitude in peak flux. The physical picture that arises is that solar flares are avalanches of many small reconnection events, analogous to avalanches of sand in the models published by Bak and colleagues in 1987 and 1988. Flares of all sizes are manifestations of the same physical processes, where the size of a given flare is determined by the number of elementary reconnection events. The relation between small-scale processes and the statistics of global-flare properties which follows from the self-organized magnetic-field configuration provides a way to learn about the physics of the unobservable small-scale reconnection processes. A simple lattice-reconnection model is presented which is consistent with the observed flare statistics. The implications for coronal heating are discussed and some observational tests of this picture are given."* This seminal paper has been cited over 300 times at the time of writing, which documents what a far-reaching impact this interpretation had in the area of solar physics alone.

Modeling of SOC behavior in solar flares started first with classical Bak–Tang–Wiesenfeld (BTW) and modified cellular automaton models (Lu and Hamilton 1991; Lu et al. 1993; Lu 1995a; Georgoulis et al. 1995, 2001; MacKinnon et al. 1996, 1997; Georgoulis and Vlahos 1998; Macpherson and MacKinnon 1999; Charbonneau et al. 2001; Belanger et al. 2007; Morales and Charbonneau 2008a,b, 2009). Alternatively, also a continuously

Table 1.6 SOC in solar physics: Observations of solar flare phenomena with powerlaw-like event occurrence frequency distributions.

Phenomenon:	Selected references:
flare gamma rays:	Perez-Enriquez and Miroshnichenko (1999)
flare hard X-rays:	Datlowe et al. (1974) Dennis (1985) Schwartz et al. (1992) Crosby et al. (1993, 1998, 1999) Lu et al. (1993) Lee et al. (1993) Bromund et al. (1995) Aschwanden et al. (1995, 1998b) Kucera et al. (1997)
microflare hard X-rays:	Lin et al. (1984, 2001) Biesecker et al. (1993, 1994) Su et al. (2006) Christe et al. (2008)
flare soft X-rays:	Hudson et al. (1969) Drake (1971) Shimizu (1995) Lee et al. (1995) Feldman et al. (1997) Veronig et al. (2002a,b) Das et al. (2004) Yashiro et al. (2006)
microflare soft X-rays:	Shimojo and Shibata (1999)
nanoflare EUV emission:	Krucker and Benz (1998) Aschwanden et al. (2000a) Aletti et al. (2000) Benz and Krucker (2002) Aschwanden and Parnell (2002)
flare ultraviolet emission:	Nishizuka et al. (2009)
chromospheric events Hα:	Georgoulis et al. (2002)
flare radio emission:	Akabane (1956) Kundu (1965) Kakinuma et al. (1969) Fitzenreiter et al. (1976) Aschwanden et al. (1995, 1998b) Mercier and Trottet (1997) Das et al. (1997) Meszarosova et al. (1999) Melendez et al. (1999) Nita et al. (2002, 2004) Ning et al. (2007)
solar energetic particles events (SEP):	VanHollebeke et al. (1975) Cliver et al. (1991) Gabriel and Feynman (1996) Miroshnichenko et al. (2001) Gerontidou et al. (2002)

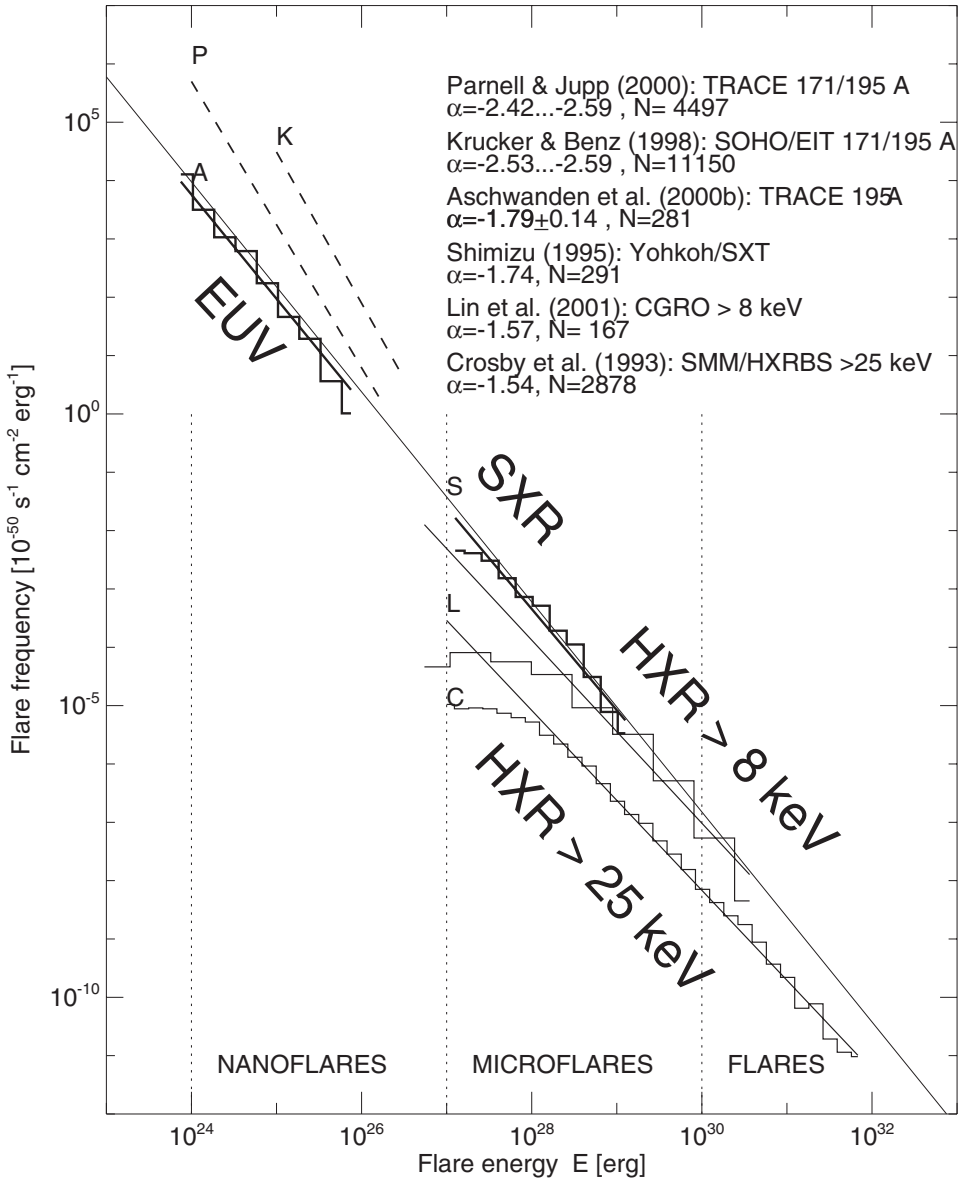

Fig. 1.14 Composite flare frequency distribution in a normalized scale in units of 10^{-50} flares per time unit (s^{-1}), area unit (cm^{-2}), and energy unit (erg^{-1}). The energy is defined in terms of thermal energy $E_{th} = 3n_e k_B T_e V$ for extreme ultraviolet (EUV) and soft X-rays (SXR), and in terms of nonthermal energy in >25 keV (Crosby et al. 1993) or >8 keV electrons (Lin et al. 2001). The slope of −1.8 is extended over the entire energy domain of 10^{24}–10^{32} erg. The offset between the two hard X-ray (HXR) datasets is attributed to different lower energy cutoffs as well as different levels of flare activity during the observed time intervals (adapted from Aschwanden et al. 2000b; Lin et al. 2001).

driven Olami–Feder–Christensen (OFC) model has been applied to solar flares (Hamon et al. 2002). However, although cellular automaton models can reproduce SOC behavior in the form of powerlaw distributions, no particular physics is attached to cellular automaton models, which seem to have some universal characteristics. On the next level, modelers attempted to incorporate physics-based models, such as linking discretized MHD equations to the next-neighbor interactions of cellular automaton models (Vassiliadis et al. 1998; Isliker et al. 2001; Galtier and Pouquet 1998) or MHD simulations (Galsgaard 1996). Along the same line of thought, MHD turbulence and associated heating was linked to SOC models (Walsh et al. 1997; Dmitruk and Gomez 1997; Dmitruk et al. 1998; Boffetta et al. 1999; Liu et al. 2002; Krasnoselskikh et al. 2002). Other physics-based SOC lattice models include particle acceleration in random DC electric fields (Anastasiadis et al. 1997), the scaling of energy release with the magnetic field, i.e., $E \propto B^2$ (Vlahos 2002; Vlahos et al. 2002; Vlahos and Georgoulis 2004), magnetic helicity dissipation (Chou 1999, 2001), chromospheric evaporation (Mitra-Kraev and Benz 2001), annihilation of magnetic elements (Podlazov and Osokin 2002), or cascades of magnetic reconnections (Hughes et al. 2003).

Most existing SOC models are based on lattice grids, where avalanches are created by next-neighbor interactions triggered above a critical threshold, which can be formulated by mathematical rules and rendered by numerical simulations. In contrast to these lattice-type models, the probability distributions of SOC models can also be calculated by analytical means, using parameterized distributions and differential equations to describe the dynamics of a physical process in a SOC avalanche event. Such analytical SOC models have been developed in terms of logistic avalanches (Aschwanden et al. 1998b), master equations (Wheatland and Glukhov 1998; Litvinenko and Wheatland 2001; Wheatland 2009), magnetic separator reconnection models (Litvinenko 1996, 1998a,b; Longcope and Noonan 2000; Litvinenko and Wheatland 2001; Wheatland 2002; Craig and Wheatland 2002; Wheatland and Craig 2003), or torsional Alfvén waves (Wheatland and Uchida 1999). We will discuss physics-based SOC models of solar flares in more detail in Chapter 9.

1.9 SOC in Stellar Physics

Stellar coronae must be governed by similar physics as we observe in the solar corona, especially for stars with similar strong magnetic fields, and similar temperatures and rotation rates. Flares are ubiquitous among coronal stars and have been observed from almost the entire main sequence and giants (e.g., see review by Güdel (2004)). Very energetic flares are frequently seen in ultraviolet, soft X-ray, and radio wavelengths from red dwarf stars of the dMe class, such as from AD Leo, AT Mic, AU Mic, EV Lac, UV Cet, or YZ CMi. Stellar observers started to gather statistics of flare events detected during an observational run and found similar powerlaw distributions as for solar flares, and thus interpreted them in terms of SOC behavior. Powerlaw distributions have been found for stellar flares with the following (noncumulative) slopes: $\alpha = 2.25 \pm 0.1$ for YZ CMi (Robinson et al. 1999), $\alpha \approx 1.6$–2.4 for 12 type F to M stars (Audard et al. 2000), $\alpha \approx 2.0$–2.7 for FK Aqr, V1054 Oph, and AD Leo (Kashyap et al. 2002), or $\alpha \approx 2.3 \pm 0.1$ for AD Leo (Arzner and Güdel 2004).

A synopsis of the dataset of 12 flare stars observed by Audard et al. (2000) is shown in Fig. 1.15 and is compared with the statistics of some 19,000 solar flares observed with RHESSI, all normalized to the same energy definition (in terms of total radiated energy). We see that the largest stellar flares observed from each star have all a larger total energy than the largest solar flares, in excess of up to 3 orders of magnitude. While solar flares have been observed up to maximum energies of $E \lesssim 10^{32}$ ergs, stellar flares range up to $E \lesssim 10^{35}$ ergs (e.g., for HD 2756, a class F2 V type star). This does not mean that stellar flares of the size of solar flares do not exist, but their detection is mainly limited by the instrumental sensitivity of the detectors. The distances to the stars indicated in Fig. 1.15 run from 2.4 pc (CN Leo) to 45 pc (HD 2726). Since 1 pc is about a 200,000 times larger distance than 1 AU, this means that the flux of the largest solar flares would be a factor of 11–14 orders of magnitude fainter at those stellar distances. For the most distant star of this sample, a 10^{12} times larger sensitivity is therefore required to detected the weakest flare on this star shown in Fig. 1.15, which is still a factor of 100 brighter than the largest solar flare.

Another oddity of stellar flare frequency distributions is their systematically steeper slope ($\alpha \gtrsim 2$) than their solar counterparts ($\alpha \lesssim 2$). However, we have to be aware that most of the samples of stellar flares are obtained during a very restricted observing time interval in the order of hours, which typically includes only $n \approx 5$–15 events per star (Audard et al. 2000). The small-number statistics suggests that only the upper cutoff part of a frequency distribution is sampled, which often shows an exponential drop-off, while the powerlaw part is usually manifest when the distribution extends over a larger inertial range (i.e., the powerlaw part of the distribution), say over at least two orders of magnitude (Aschwanden 2007). The distribution of solar flares (from RHESSI) that extends over almost 5 orders of magnitude shown in Fig. 1.15 demonstrates this point: a powerlaw-like part is seen in the lower 4 orders of magnitude in energy, while an exponential drop-off is apparent at the high-energy end, probably limited by the maximum active region size (Kucera et al. 1997). Thus, the systematic difference in observed powerlaw slopes may be mostly an observational limitation, rather than a fundamental difference in the physics of flares on the Sun and stars, and thus may not provide a valid argument for the dominance of coronal heating by nanoflares (which requires a powerlaw slope of steeper than 2; Hudson (1991)).

Theoretical interpretations of stellar flare observations in terms of SOC behavior range from superposition of stochastic flaring and heating events (Arzner and Güdel 2004), to self-regulation of the coronal density driven by chromospheric evaporation and radiative cooling (Uzdensky 2007), or self-driving embedded Sweet–Parker reconnection (Cassak et al. 2008).

Cataclysmic variable stars (CV) are stars that exhibit irregular brightness variations, with quiescent time intervals in between. Over 1,600 CV systems are known today. The interpretation for these episodic bursts is thought to be a mass transfer between close binary stars (Fig. 1.16), consisting of a white dwarf primary star and a secondary star with an orbital period in the range of $P \approx 1$–10 hours. Gravitational disturbances of the primary dwarf star on the secondary star (the donor star) can trigger infall of matter that is accreted in the primary star, leading to an accretion disk around the dwarf star. Occasional instabilities in the accretion disks lead to X-ray bursts whenever an avalanche of unstable massis

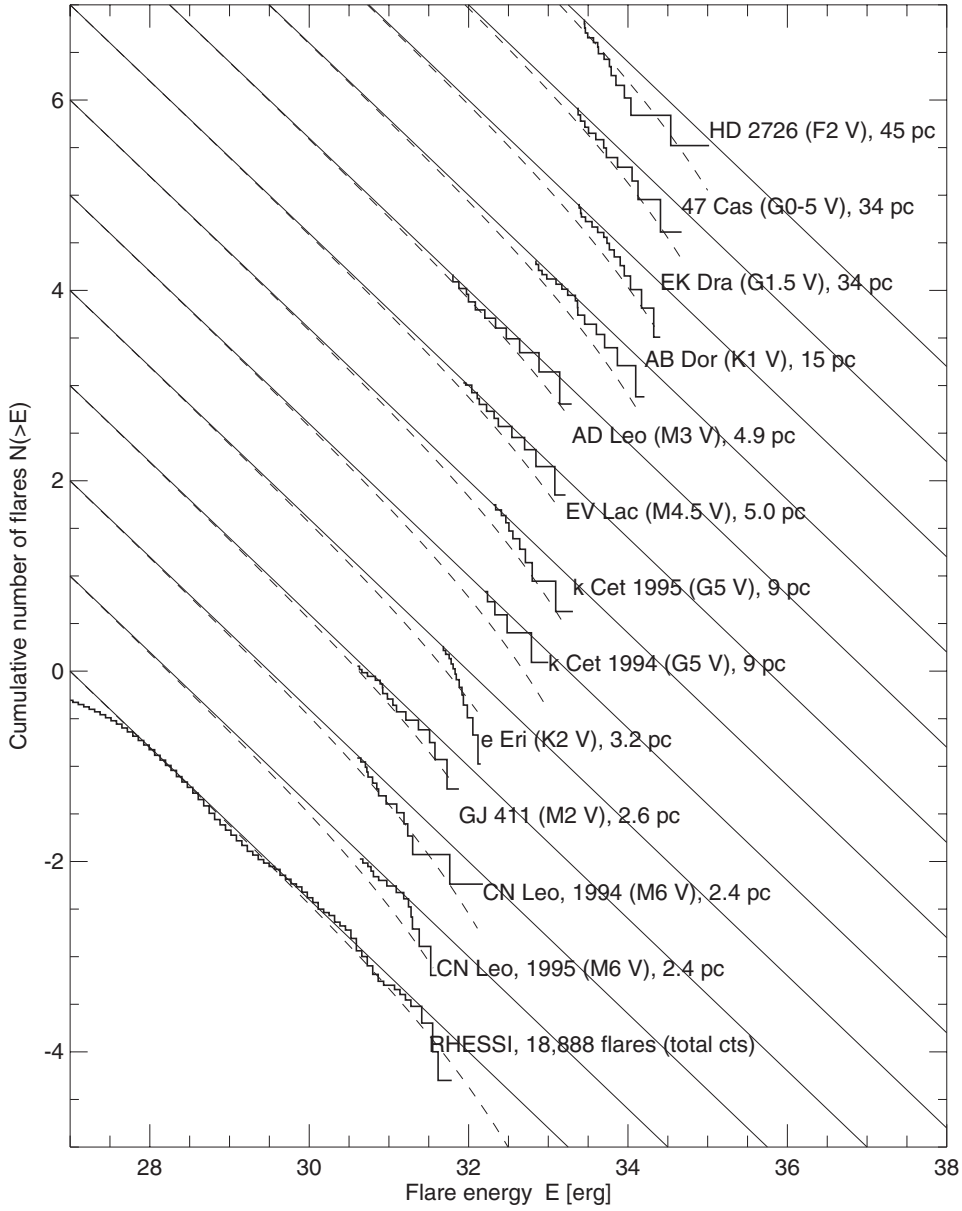

Fig. 1.15 Cumulative occurrence frequency distributions $N(>E)$ of stellar flares (vertically shifted for each star, in order of stellar distance) are shown as a function of the flare energy E, observed from 12 different stars by Audard et al. (2000). For comparison we show also the statistics of total hard X-ray emission of 18,888 solar flares observed with RHESSI, which covers an energy range of $E \approx 10^{27.0}$–$10^{31.7}$ ergs, while stellar flares have an energy range of $E \approx 10^{30.7}$–$10^{35.0}$ ergs. Note that most distributions show a (cumulative) powerlaw part with a slope of $\alpha \approx 0.8$ (diagonal lines) at the low end and an exponential high-energy drop-off. The distributions are incrementally shifted for clarity.

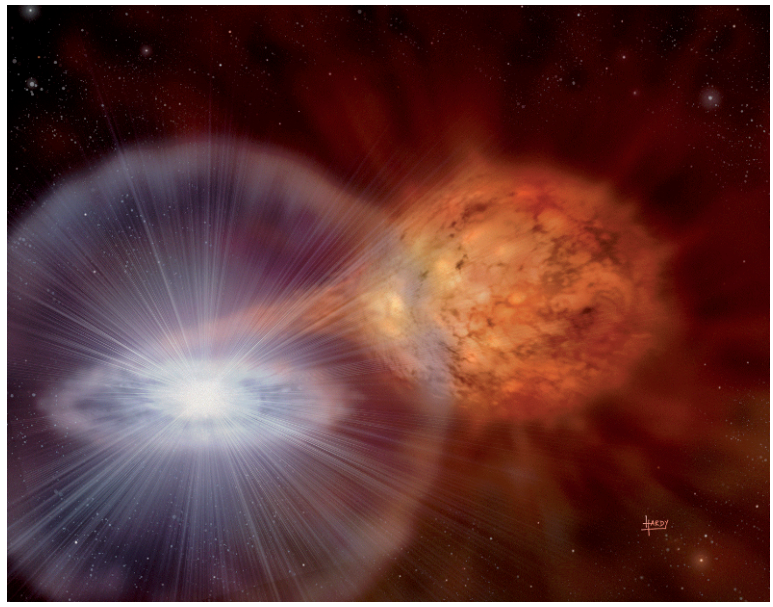

Fig. 1.16 Artistic rendering of the cataclysmic variable star RS Ophiuchi, which exhibits a nova outburst about every 20 years. This binary system contains a white dwarf and a red giant with mass transfer (credit: PPARC, David A. Hardy).

hurled inward. Even larger instabilities can produce nova outbursts, whenever the density and temperature raises above a critical threshold to ignite nuclear fusion reaction.

Optical emission from CVs or accretion disks exhibits short rapid random variability, called "flickering". The power spectral density $S(f)$ as a function of the frequency f was found to have a powerlaw behavior, i.e., $S(f) \propto f^{-1\ldots-2}$ (Bruch 1992, 1995; Kato et al. 2002), and thus was interpreted in terms of SOC systems (Mineshige et al. 1994a; Dendy et al. 1998; Wiita and Xiong 1998; Mineshige 1999). The waiting-time distribution of rapid fluctuations in X-rays from Cygnus X-1 was found to be exponential (Negoro et al. 1995), implying a random process that can be modeled with a shot-noise model (Negoro et al. 1995; Focke 1998). Massive CVs with accretion disks can form black holes, where the gravitational field is so powerful that it even traps light and precludes escape. The evolution of a black hole thus involves also accretion disks, for which SOC behavior is postulated, similarly to other accretion disk systems (Sivron 1998; Mineshige and Negoro 1999; Xiong et al. 2000). Modeling of the SOC behavior in terms of cellular automaton models was conducted and could reproduce the power spectrum characteristics of the flicker noise of cataclysmic variables (Yonehara et al. 1997; Takeuchi and Mineshige 1997; Pavlidou et al. 2001) or black holes (Takeuchi et al. 1995).

Pulsars are highly magnetized, rotating neutron stars, exhibiting short periods in the range of 1.4 ms to 8.5 s. The most famous one is the Crab pulsar with a period of 33 ms. Although pulsars rotate with such a high precision that they are used as timekeepers, there are some glitches observed occasionally, which are related to the superfluidity and

superconductivity inside the star that allows the neutrons to flow without friction (Pizzochero et al. 1997). The probability of pulsar glitches as function of the glitch energy was found to be a powerlaw, i.e., $P(E) \propto E^{-3.5}$ (Argyle and Gower 1972; Lundgren et al. 1995), $P(E) \propto E^{-1.14}$ (Morley and Garcia-Pelayo 1993), $P(E) \propto E^{-2.8}$ (Cognard et al. 1996), which has been related to a SOC system (Young and Kenny 1996). Modeling of pulsar glitches has been conducted in terms of electric fields, for which a powerlaw-like probability distribution of $P(E) \propto E^{-4.6\ldots-9}$ was found (Cairns 2004; Cairns et al. 2004). A cellular automaton model of pulsar glitches was constructed based on the superfluid vortex unpinning paradigm (Warzawski and Melatos 2008; Melatos et al. 2008).

A related class is the soft gamma repeater (SGR), an object that shows a repetitive emission of low-energy gamma-ray bursts. SGRs have been interpreted in terms of starquakes, which are the result of a fracture of the crust of a magnetically powered neutron star or "magnetar" (Duncan and Thompson 1992; Thompson and Duncan 1996). The fluence distribution of SGR bursts was found to have a powerlaw with slopes of $\alpha \approx 1.4$–1.7 (Gogus et al. 1999, 2000), and thus has been associated with SOC behavior like earthquakes, and hence, called starquakes. A compilation of references for SOC phenomena in stellar physics is given in Table 1.7.

1.10 SOC in Galaxies and Cosmology

On galactic scales, X-ray variability has been observed in so-called *active galactic nuclei (AGN)*, which often are radio galaxies or blazars. Physical interpretations attributed to such X-ray variability are X-ray jets, disk-corona models where X-ray emission originates from comptonization of soft UV thermal photons, or black hole models. An X-ray light curve analysis of a radio galaxy was found to be consistent with shot-noise statistics, which lends to the same SOC interpretation as for the black hole candidate Cygnus X-1 (Leighly and O'Brien 1997; Ciprini et al. 2003).

Cosmic structures at large scales, such as galactic spirals and galaxy clusters, display complex and fractal geometries (although the universe turns over to being remarkably homogeneous and isotropic at cosmological scales of the microwave background). Since fractals are scale-free, as self-organized criticality leads to scale-free spatial and temporal structures, SOC behavior could also play a role in the creation of large-scale structures in the universe, not requiring any fine tuning to achieve a critical state. Although a full SOC model has not been developed yet for structures in the early universe, self-organization and fractal scaling (which is SOC without criticality) has already been applied to some large-scale structures, such as to the formation of the interstellar medium (Tainaka et al. 1993), the galactic spiral structure (Nozakura and Ikeuchi 1988), the stellar dynamics in elliptical galaxy formation (Kalapotharakos et al. 2004), or the initial mass function of starbursts (Melnick and Selman 2000), or gravitational structure formation in general on many scales (Da Rocha and Nottale 2003). In numerical N-body simulations of elliptical galaxy formation it is found that the initial chaotic orbits become ordered as the short axis tube type during their evolution, which is a self-organization process (Kalapotharakos et al. 2004),

What about SOC and cosmology? Although the following excerpt is not mainstream cosmology, it contains intriguing thoughts about the possible application of SOC to cos-

Table 1.7 SOC behavior in stellar physics: The references include observational and theoretical modeling papers.

Phenomenon	References
stellar flares	Robinson et al. (1999) Audard et al. (2000) Kashyap et al. (2002) Arzner and Güdel (2004)
cataclysmic variable (CV) stars	Bruch (1992, 1995) Yonehara et al. (1997) Takeuchi and Mineshige (1997) Kato et al. (2002)
accretion disks	Dendy et al. (1998) Wiita and Xiong (1998) Mineshige (1999) Xiong et al. (2000) Pavlidou et al. (2001)
black holes	Mineshige et al. (1994a) Takeuchi et al. (1995) Sivron (1998) Mineshige and Negoro (1999)
pulsar glitches	Argyle and Gower (1972) Morley and Garcia-Pelayo (1993) Cognard et al. (1996) Lundgren et al. (1995) Young and Kenny (1996) Cairns (2004) Cairns et al. (2004) Warzawski and Melatos (2008) Melatos et al. (2008)
soft gamma repeaters (SGR)	Duncan and Thompson (1992) Thompson and Duncan (1996) Gogus et al. (1999, 2000)

mology. We quote from Moffat (1997): *A major problem in modern cosmology is this: How could the universe evolve during more than 10 Gyr and become so close to spatial flatness and avoid the horizon problem? Why is the universe so homogeneous and isotropic? How could such a critical state of the universe come about without a severe fine tuning of parameters. The usual explanation for these questions is based on the idea of inflation. However, inflation is a type of phenomenon that in statistical mechanics corresponds to the existence of an attractor that requires fine tuning of the parameters.* Moffat (1997) then proposes that the universe evolves as a SOC system (in the sense of the Bak-Tang-Wiesenfeld model) with the Hubble expansion undergoing "punctuated equilibria" with energy being dissipated at all scales. Note that punctuated equilibria involve a number of episodic bursts, separated by time intervals of near steady-state, so the implication is that there occurred many inflation phases in the past, not just one. A consequence is

Table 1.8 SOC concepts in galaxies and cosmology.

Phenomenon	References
active galactic nuclei, blazars	Leighly and O'Brien (1997) Ciprini et al. (2003)
interstellar medium formation	Tainaka et al. (1993)
galactic spiral structure	Nozakura and Ikeuchi (1988)
elliptical galaxy formation	Kalapotharakos et al. (2004)
IMF of starbursts	Melnick and Selman (2000)
gravitational structure formation	Da Rocha and Nottale (2003)
cosmology, big bang, inflation	Moffat (1997)
quantum gravity	Ansari and Smolin (2008)

that the SOC model predicts a critical value for the density profile, $\Omega = 1$, which is the critical value between an open ($\Omega_c \leq 1$) or closed universe, independent of the initial conditions and without fine tuning of the parameters. *The metric fluctuations display 1/f flicker noise, correlations of fluctuations occur at all length scales, and the universe evolves at the "edge of chaos". There is only one possible stable choice (i.e., stable under local perturbations) for the present expanding universe whatever its initial conditions. According to our assumptions the space-time geometry fluctuates randomly at some length scale. If we assume that the metric fluctuations are very intense at the beginning of the universe, and that they smear out the light cones locally, then for a given short duration of time Δt after the big-bang there will be communication of information "instantaneously" throughout the universe. This will resolve the "horizon" problem and explain the high degree of isotropy and homogeneity of the present universe* (Moffat 1997). A related SOC concept has also been applied to quantum gravity (Ansari and Smolin 2008). A few references to SOC concepts applied to galaxies and cosmology are given in Table 1.8.

1.11 Summary

Self-Organized Criticality (SOC) is a theoretical concept that describes the statistics of nonlinear processes. It is a fundamental principle that is common to many nonlinear dissipative systems in the universe. Due to its universality and ubiquity, SOC is a law of nature, for which we derive the theoretical framework and specific physical models in this book. The SOC concept was introduced by Bak, Tang, and Wiesenfeld in 1987 and has been applied to laboratory experiments of sandpiles, to human activities such as population growth, language, economy, traffic jams, or wars, to biophysics, geophysics (earthquakes, landslides, forest fires), magnetospheric physics, solar physics (flares), stellar physics (flares, cataclysmic variables, accretion disks, black holes, pulsar glitches, gamma ray bursts), and to galactic physics and cosmology. From an observational point of view, the hallmark of SOC behavior is the powerlaw shape of occurrence frequency distributions of spatial, temporal, and energy scales, implying scale-free nonlinear processes. Powerlaws are a necessary but not sufficient condition for SOC behavior, because intermittent turbulence also produces powerlaws. While we surveyed the manifestation of SOC behav-

ior from "microscopic" scales (sandpiles) across the universe out to cosmological scales in this introductory chapter, as documented in the literature of some 1,000 research publications, we will provide a more detailed introduction into the theoretical concepts, modeling, and interpretation of SOC behavior in the following chapters.

1.12 Problems

Problem 1.1: Count the words of an English text, either visually or with some computer program (e.g., http://www.hermetic.ch/index.php), and plot the frequency of words in a rank-ordered Zipf plot (similar to the graph in Fig. 1.4 right panel for city sizes). Do you obtain the same order of words as it is found for the English language in general? The first 15 words, in order of frequency, are: *"the", "of", "and", "in", "to", "a", "is", "that", "it", "as", "this", "by", "for", "be", "not"*.

Problem 1.2: How are rank-ordered plots, cumulative frequency distributions, and noncumulative (differential) frequency distributions related to each other? Derive a mathematical proof that a powerlaw in a rank-ordered plot corresponds to a powerlaw of a cumulative frequency distribution. What is the difference in the powerlaw slope between a cumulative and noncumulative frequency distribution? (Check your answers in Section 7.1.)

Problem 1.3: Is there a concentration or preferred range of powerlaw slopes α of (noncumulative) occurrence frequency distributions? (Hint: Plot a histogram of the values quoted in Chapter 1.)